Solid State Communications 150 (2010) 1009–1022

Contents lists available at ScienceDirect

Solid State Communications

journal homepage: www.elsevier.com/locate/ssc

Review of mathematical models for biofilms

Qi Wang [a], Tianyu Zhang [b,*]

[a] Department of Mathematics and NanoCenter at USC, University of South Carolina, Columbia, SC 29208, United States
[b] Department of Mathematical Sciences, Montana State University, Bozeman, MT 59717, United States

ARTICLE INFO

Article history:
Received 24 July 2009
Accepted 11 November 2009
by the Guest Editors
Available online 29 January 2010

Keywords:
A. Biofilms
C. Mathematical models

ABSTRACT

In this paper, we briefly review the progress made in the mathematical modeling of biofilms over the last 30 years. Biofilms constitute a spectrum of dynamical microorganisms, whose interaction with the surrounding environment and thereby induced dynamics dictates the complex properties of the living organism. Modeling of biofilms began with a low dimensional continuum description first based on kinematics and translational diffusions; later, more sophisticated microscopic dynamical mechanisms are introduced leading to the anomalous diffusion and dissipation encountered by various components in biofilms. Recently, biofilm and bulk fluid (or solvent) coupling has been investigated using discrete-continuum, multifluid and single fluid multicomponent models to treat the entire biofilm-bulk-fluid system either as a system consisting of various components whose dynamics exhibits different time scale or as a whole. We classify the models into roughly four classes: low-dimensional continuum models, diffusion limited aggregation models, continuum-discrete models, and fully coupled biofilm-fluid models. We will address some hybrid models that combine the ideas from the above categories and new computational protocols combining the existing computational tools for cell dynamics coupled with the discrete-continuum biofilm model.

1. Introduction

Biofilms are ubiquitous in natural and industrial settings. The development of biofilms is a multistage process. First, free floating planktonic bacterial cells land on a damp surface and later get attached to it. After a sufficiently high cell density is reached, cells begin excreting an extracellular polymeric substance (EPS) and forming a EPS matrix anchored on the surface. The bacteria population inside the matrix grows as well by consuming nutritious substrates supplied by the surrounding environment. As the result, the biofilm begins to grow. Biofilm growth is a dynamical process whose structure is largely influenced by environmental conditions including the substrate diffusion limitation and the shear stress of the bulk fluid. Biofilms generally consist of multispecies of bacteria, as well as fungi, algae, yeasts, protozoa, other microorganisms, debris, corrosion products, EPS and solvent (water). All these components are held together by the EPS to form a complex heterogeneous dynamical bio-organism.

Biofilm related problems cost the US literally billions of dollars every year in energy losses, equipment damage, product contamination and medical infections. But biofilms also offer a huge potential for bio-remediating hazardous waste sites, bio-filtering municipal and industrial water and waste water, forming bio-barriers to protect soil and ground water from contamination, as well as heap leaching in the mining industry. It is important and apparently challenging to unravel the complex dynamical properties of the biofilms, prevent damage caused by unwanted biofilm growth and to utilize biofilms for good causes.

Biofilm formation is a complicated dynamical process governed by various physical, chemical principles and biological protocols. Biofilm development depends heavily on the environmental conditions and types and properties of the bacteria inside the biofilm. Bacteria in biofilms are very resistant to antimicrobial agents due to the limited penetration of antimicrobial agents. Mathematical modeling of biofilms is crucial to attain a broader and deeper understanding of this complex microorganism. The mathematical models can not only be used to verify experimental findings, but also to make qualitative and quantitative predictions that might well serve as guidelines for experimental design. There has been extensive research on the mathematical modeling of biofilms in the last three decades and there has been accumulated a very rich literature. Some of the models were proposed and applied successfully in explaining and predicting the biofilm's behavior in various conditions. Chronically, the development of the biofilm models has undergone an evolution from simple to complex, from one spatial dimensional models to multidimensional models, from single species models to

* Corresponding author. Tel.: +1 406 994 5363; fax: +1 406 994 1789.
E-mail addresses: qwang@math.sc.edu (Q. Wang), zhang@math.montana.edu (T. Zhang).

0038-1098/$ – see front matter © 2010 Elsevier Ltd. All rights reserved.
doi:10.1016/j.ssc.2010.01.021

multispecies models, from steady-state models to dynamical models, from pure growth models to models including biomass growth and biofilm–fluid interaction, from models describing a particular process to models incorporating many different processes occurring simultaneously, from qualitative models to quantitative models, and from single scale models to multiscale ones, etc.

In this article, we will give a brief review of some biofilm models developed in the past 30 years, most of which have been successfully applied to studying the biofilms' growth. We classify the models based on their dimensionality, the way in which diffusion is treated, and the complexity in terms of the incorporation of the physics, chemistry and biological effects into four main categories: one dimensional continuum models, diffusion limited aggregate models, continuum-discrete diffusion models, and biofilm–fluid coupled models. There have been several excellent review articles about biofilms from the biological, physiological, mechanical and mathematical perspectives by a group of distinguished researchers in the field [1–4]. We hope to give the review from a different perspective giving a chronological perspective on the development of various models and their mathematical structure evolution.

2. 1-dimensional continuum models

Early efforts on the mathematical modeling of biofilms can be traced back to the 1980s represented by the work of [5–10]. These authors studied biofilms using continuum models primarily in one space dimension. These studies are centered mostly on the steady-state biofilm growth dynamics including the biofilms' thickness and spatial distribution of microbial species and substrate concentration. We illustrate the idea and basic mathematical structures in these models using the multispecies biofilm model introduced by Wanner and Gujer [9] as an example. The model is based on a continuum description of the biofilms' material and conservation principles; it predicts the evolution of the biofilms' thickness, dynamics and spatial distribution of microbial species and substrates in the biofilm. It also allows a biomass detachment due to the shear stress and sloughing. Assuming that the biofilm contains nx different microbial species in a control volume between z and $z + \mathrm{d}z$ with a cross sectional area A in the support interface, a mass balance of the species i is set up for a differential volume $A\,\mathrm{d}z$ as follows (see Fig. 1)

$$\frac{\partial[A\,\mathrm{d}z\ \rho_i f_i(t,z)]}{\partial t} = A\,\mathrm{d}z\ \mu o_i(t,z)\rho_i f_i(t,z) + A g_i(t,z) - A\left[g_i(t,z) + \frac{\partial g_i(t,z)}{\partial z}\mathrm{d}z\right], \tag{2.1}$$

where ρ_i is the constant density for the i-th species, f_i denotes the volume fraction of the i-th species, μo_i is the observed specific growth rate, and g_i is the mass flux of the ith species in the z-direction, namely, the mass of the species i that is displaced per unit time and unit area across a plane transverse to the z-direction. Dividing (2.1) by $A\,\mathrm{d}z\ \rho_i$ yields the differential equation

$$\frac{\partial f_i}{\partial t} = \mu o_i f_i - \frac{1}{\rho_i}\frac{\partial g_i}{\partial z}. \tag{2.2}$$

Let $u(t,z)$ be the velocity at which the microbial mass is displaced with respect to the film-support interface, the flux g_i can be expressed as $g_i(t,z) = u(t,z)\rho_i f_i(t,z)$. Thus, (2.2) can be written as

$$\frac{\partial f_i}{\partial t} = \left(\mu o_i - \frac{\partial u}{\partial z}\right) f_i - u\frac{\partial f_i}{\partial z}. \tag{2.3}$$

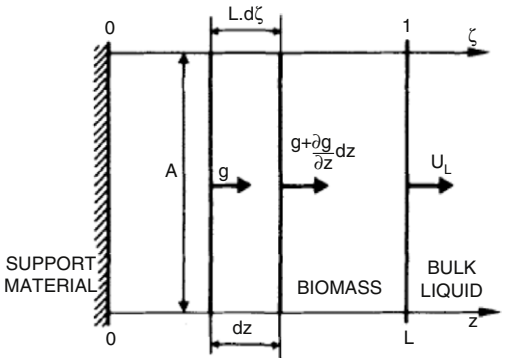

Fig. 1. Flux of biomass through a differential volume element of an expanding idealized biofilm.

Summing Eq. (2.3) over all the nx microbial species and using the sum of the volume fractions equals 1, i.e., $\sum f_i = 1$, we obtain

$$\frac{\partial u(t,z)}{\partial z} = \bar{\mu} o(t,z), \quad \text{where } \bar{\mu} o(t,z) = \sum_{i=1}^{nx} \mu o_i(t,z) f_i(t,z). \tag{2.4}$$

Thus the velocity u is determined by the mean observed specific growth rate of the biomass $\bar{\mu} o(t,z)$ by

$$u(t,z) = \int_0^z \bar{\mu} o(t,z')\mathrm{d}z', \tag{2.5}$$

where $u(t,0)$ is set to zero. We remark that this microbial mass transport velocity is identical to all species, which is clearly an artifact of the model. If the biofilm grows or shrinks, its thickness $L(t)$ changes and the film–water interface moves at a velocity $u_L(t) = \frac{\mathrm{d}L(t)}{\mathrm{d}t}$. With $\sigma(t)$ is defined as the velocity at which the biomass is exchanged between the biofilm and the bulk liquid outside the biofilm and by use of Eq. (2.5), the velocity of the film–water interface is expressed as

$$u_L(t) = u(t,L) + \sigma(t) = \int_0^L \bar{\mu} o(t,z')\mathrm{d}z' + \sigma(t).$$

In this paper, the biomass loss due to shear stress is modeled by setting $\sigma = -\lambda L^2$ with some constant λ, and the biomass loss due to sloughing is modeled by setting σ as a δ function.

Substitution of (2.4) into (2.3) yields the mass balance equation for f_i:

$$\frac{\partial f_i}{\partial t} = [\mu o_i(t,z) - \bar{\mu} o_i(t,z)] f_i(t,z) - u(t,z)\frac{\partial f_i(t,z)}{\partial z}, \quad i = 1,\ldots,nx-1. \tag{2.6}$$

Assuming that the bulk liquid contains ns different substrates, in the same way as for the microbial species, a mass balance for the substrate i is obtained

$$\frac{\partial S_i(t,z)}{\partial t} = r_i(t,z) + \frac{\partial}{\partial z}\left(D_i\frac{\partial S_i(t,z)}{\partial z}\right), \quad i = 1,\ldots,ns, \tag{2.7}$$

where S_i is the concentration, r_i the observed conversion rate, and D_i the diffusion coefficient of substrate i. The boundary conditions for the film-support interface ($z = 0$) are no-flux boundary conditions given by

$$\frac{\mathrm{d}f_i}{\mathrm{d}t} = (\mu o_i - \bar{\mu} o) f_i, \qquad \frac{\partial S_i}{\partial z} = 0.$$

For the film–water interface ($z = L$), with or without an external mass transfer limitation, the boundary conditions are defined by

$$\frac{\partial S_i}{\partial z} = \frac{LD_{l_i}}{L_l D_i}(S_{l_i} - S_i) \quad \text{or} \quad S_i = S_{l_i}$$

where L_l is the thickness of the effective substrate transfer layer between the film–water interface and the bulk liquid, D_{l_i} is the diffusion coefficient of substrate i in the bulk fluid, S_{l_i} is the concentration of substrate i in the bulk liquid. The specific growth rates μo_i and the substrate conversion rates r_i are given by monod models.

The steady-state analysis of this multispecies biofilm model predicts that for any given kinetics, the spatial distribution of a microbial species may be described by one or more layers, each being either homogeneous or mixed. Numerical solutions of the time-dependent equations were computed for 5 cases in the situation of a heterotrophic–autotrophic competition for space and for oxygen as a common substrate. The five cases are: 1. Unrestricted Growth; 2. Changes in Bulk Liquid Substrate Concentration; 3. Biomass Shear; 4. Biomass Sloughing; 5. Biofilm in a Completely Mixed Reactor with External Mass Transfer Resistance. The development of the biofilms' thickness and the removal of substrates from the bulk liquid with time are presented for each case. The model predicts how the microbial composition of the biofilm depends on the microbial kinetics, the substrate concentration as well as different reactor configurations and an alternative biomass detachment mechanism.

Based on new experimental observations, an extended mixed-culture biofilm (MCB) model was introduced by [11] later. This model includes a more flexible description of the transport of dissolved components in the biofilm and considers the diffusive transport of particulate components in the biofilm's solid matrix, changes of the biofilm's liquid phase volume fraction (porosity), and the simultaneous detachment and attachment of cells and particles at the biofilm's surface. This extended model can reproduce most of the new experimental data. This model is derived based on the general mass conservation principle and is independent of any special set-up except for limitations in one space dimension. The model can be adjusted to any specific microbial kinetics or biomass detachment mechanism, and used to predict the short and long term behavior of the biofilm's growth. Indeed the model has been successfully applied to many biofilm studies since its development, and it has helped enormously in understanding the complex bulk interactions in the multispecies biofilms. On the other hand, since it is a one-dimensional model, it significantly simplifies the interaction between the substrate and the biofilm and the spatial dynamics of the biofilm. It also lacks the ability to characterize the multidimentional morphology of the biofilm. Various higher dimensional models with a biofilm–flow interaction are developed later.

3. DLA model for biofilm growth and pattern formation

In general the growth mechanism of the bacterial colonies is highly complex, in which the substrate concentration plays an important role. One way to model the growth pattern is through the class of models called the diffusion-limited aggregation (DLA) model. The DLA growth was first studied through computer simulations [12] and the first biological DLA example was a DLA colony of *Bacillus subtilis* given by [13]. More experimental and modeling work was done in [14,15] later. The rule of the DLA model is as follows: one chooses a seed particle as the origin of a square lattice on a plane. Another particle is released far from the origin and is allowed to move at random. When it arrives at the nearest neighboring site to the origin, it sticks to the site. Then another particle is launched and it moves until it reaches the nearest neighboring site of a cluster made of the two particles. Through the repetition of these procedures, a cluster grows with an outwardly open and randomly branched structure as shown by a computer simulation in (Fig. 2(b)) [16]. Its pattern is morphologically self-similar, implying that it is a fractal.

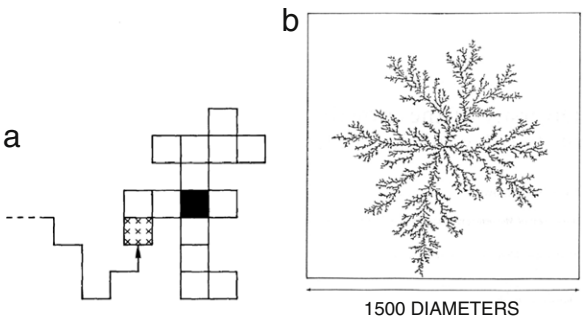

Fig. 2. DLA on computer simulation: (a) the rule of the 2D DLA growth. The solid cell is the origin. The hatched cell is a new cell that has aggregated to the cluster; (b) a typical example of a 2D DLA cluster which consists of 100,000 particles.

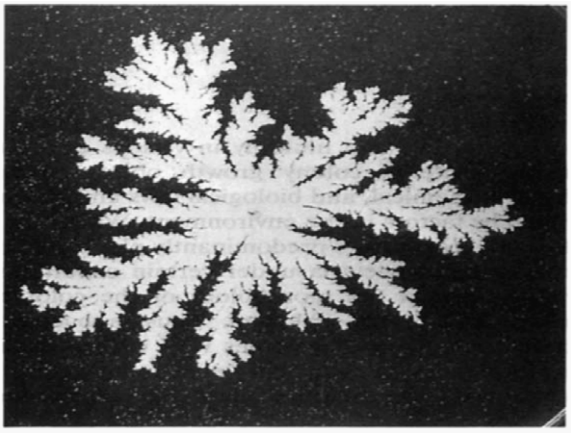

Fig. 3. An example of a DLA colony. The colony was photographed 21 days after inoculation. Its diameter was about 47 mm.

Fig. 3 [15] shows the morphology of a *B. subtilis* strain that grows through the DLA process at a very low nutrient level on an agar plate. The colony had an outwardly open and randomly branched structure, and these findings were in good agreement with the computer simulations of the DLA model. This suggests that *B. subtilis* cells grow predominantly obeying a simple physical law, diffusion, at low limit of the nutrient concentration. A study in [15] also shows that a smoother morphology was developed under a higher nutrient concentration.

4. Discrete-continuum/Cellular Automaton (CA) model

One of the origins of the Cellular Automaton (CA) model is Conway's Game of Life [17]. It consists of a regular grid of cells, each in one of a finite number of states. The grid can be in any finite number of dimensions. Time is also discrete, and the state of a cell at time t is a function of the states of a finite number of cells (called its neighborhood) at time $t - 1$. Every cell has the same rule for updating, based on the values in this neighborhood. Each time the rules are applied to the whole grid, a new generation is created. A clear advantage of the CA model is that it can produce a complex behavior despite its simplicity, and this makes it particularly attractive to simulate biological systems which often exhibit complex spatial structures [18–20].

CA models for biofilms incorporating the biological rules including the bacterial reproduction and movement, the cell to cell communication, and the diffusion of the nutrient were extensively studied in [21–26]. These models can capture various biofilm growth patterns observed in experiments, and strongly suggest that the biofilm's structure is largely determined by the surrounding substrate concentration. [24] claims that the three

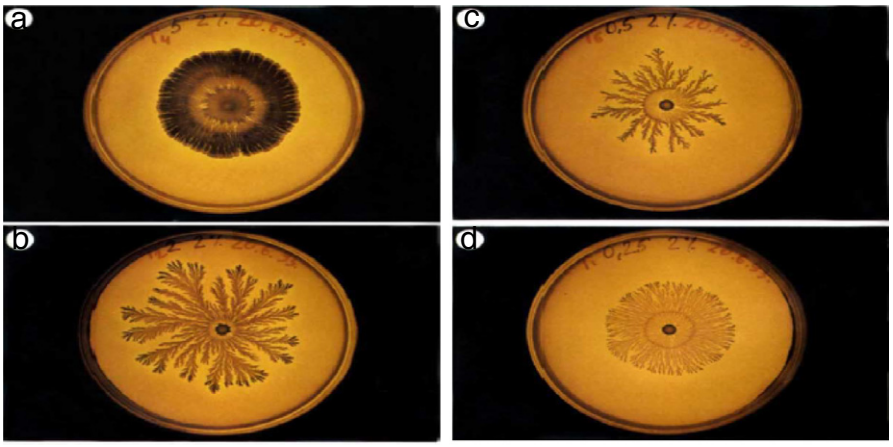

Fig. 4. Observed patterns of colonies growth on a substrate with 2% agar concentration. The peptone level is 5, 2, 0.5 and 0.25 gl^{-1} for a, b, c, d respectively.

widely accepted conceptual models of the biofilm's structure: (i) penetrated water-channel biofilm, (ii) heterogeneous mosaic biofilm, (iii) dense confluent biofilm, can all be reproduced by CA models at very different substrate concentrations.

We use the model in [23] as a representative of this class of models. The nutrient concentration $c(\vec{\mathbf{r}}, t)$ at the position $\vec{\mathbf{r}}$ and the time t is governed by the diffusion-reaction equation on a triangular lattice

$$\frac{\partial c(\vec{\mathbf{r}}, t)}{\partial t} = D_c \nabla^2 c(\vec{\mathbf{r}}, t) - \sum_{\text{active walkers}} \delta(\vec{\mathbf{r}} - \vec{\mathbf{r}}_i) \min(c_r, c(\vec{\mathbf{r}}, t)),$$

where D_c is the diffusivity for the nutrient and $\delta(\mathbf{r})$ is the Kronecker symbol. The second term on the right represents the consumption of the nutrient. A mesoscopic unit of the bacterial cells called a 'walker' is characterized by its location $\vec{\mathbf{r}}_i$ and 'internal energy' W_i which affects its activity. The walker loses the 'internal energy' at a fixed rate e and increases it through consuming nutrients at a fixed rate c_r if sufficient nutrient is available. Otherwise, it consumes the available amount. Wherever W_i drops to zero, the walker becomes stationery (sporulation). When nutrient is sufficient, W_i increases; and when it reaches some threshold t_r, the walker divides into two. The equation for the internal energy W_i is

$$\frac{\mathrm{d}W_i}{\mathrm{d}t} = \min(c_r, c(\vec{\mathbf{r}}_i, t)) - e.$$

The walkers perform an off-lattice random walk within a well defined envelope on the triangular lattice. At each time step, the random walk is of size d at an random angle Θ, uniformly chosen from $[0, 2\pi]$. The new location $\vec{\mathbf{r}}_i'$ is given by

$$\vec{\mathbf{r}}_i' = \vec{\mathbf{r}}_i + d(\cos\Theta, \sin\Theta).$$

If the step $\vec{\mathbf{r}}_i \to \vec{\mathbf{r}}_i'$ crosses the envelope, the step is not performed and a counter on the appropriate segment of the envelope is increased by 1. When a segment counter reaches N_c, the envelope segment is shifted by one lattice step. Here the level of N_c represents the agar concentration, as more 'collisions' are needed to push the envelope on a harder substrate.

Numerical results from [23] are shown in Fig. 5(a). The growth patterns are compact at high peptone levels and become fractal with decreasing food level. At a given peptone level, the patterns are more ramified as the agar concentration increases. The results capture the experimentally observed patterns shown in Fig. 4 (also from [23]) very well except that there is a discrepancy at very low peptone levels. When the nutrient concentration is low, the observed growth patterns (Fig. 4(d)) become denser again, but the simulation result (Fig. 5(a) with small P value) does not capture this feature.

The explanation of the denser pattern at a low nutrient level is that as the environmental conditions become more hostile, a higher level of cooperation is required for a more efficient response of the colony. Non-local communication between different colonies might be necessary. A chemotactic mechanism is introduced in [23] to achieve this information exchange between colonies. Generally chemotaxis means a movement of the microorganisms in response to the concentration gradient of certain chemicals. In the modified CA model, each stationary walker produces a communication chemical s at a fixed rate s_r, and each active walker consumes the chemical at a fixed rate c_c. Thus s is governed by the following reaction-diffusion equation

$$\frac{\partial s(\vec{\mathbf{r}}, t)}{\partial t} = D_s \nabla^2 s(\vec{\mathbf{r}}, t) + \sum_{\text{stationary walkers}} \delta(\vec{\mathbf{r}} - \vec{\mathbf{r}}_i) s_r - \sum_{\text{active walkers}} \delta(\vec{\mathbf{r}} - \vec{\mathbf{r}}_i) \min(c_c, s(\vec{\mathbf{r}}, t)),$$

where D_s is the diffusivity of the communication chemical. The movement of the active walker changes from a pure random walk to a random walk with a bias along the gradient of the communication field (high probability to move in the direction of the signaling material). Fig. 5(b) shows the simulation result with chemotaxis included in the model. The pattern has a denser structure with thin branches and a well defined circular envelope, and the number of walkers (bacteria density) in the colony is much lower than in the absence of chemotaxis. It is also found that a chemotactic response to the nutrient concentration gradient does not produce this effect, thus it confirms that the communication between different colonies is crucial for this growth feature.

Their apparent simplicity and great success in capturing the biofilm's structure makes the CA models very attractive. The model described above is a close approximation to the molecular diffusion in a much coarser scale. The coarseness emphasizes the stochastic nature of the model which is the main mechanism of producing a heterogeneous biofilm's morphology.

[27] developed a combined differential-discrete CA biofilm model. In this model, the substrate concentration was assumed to be continuous and governed by the conventional diffusion–reaction equation. The biomass density was computed by a direct integration of the biomass balance equation, taking into account only the growth as a result of substrate consumption. The biomass spreading was modeled by CA model. But instead of performing an entirely random walk for the "walkers", the newly formed biomass finds a place by "pushing" its neighbors to an adjacent, unoccupied space. Numerical simulations evolving in real time were carried out for both 2D and 3D, and the calculated values

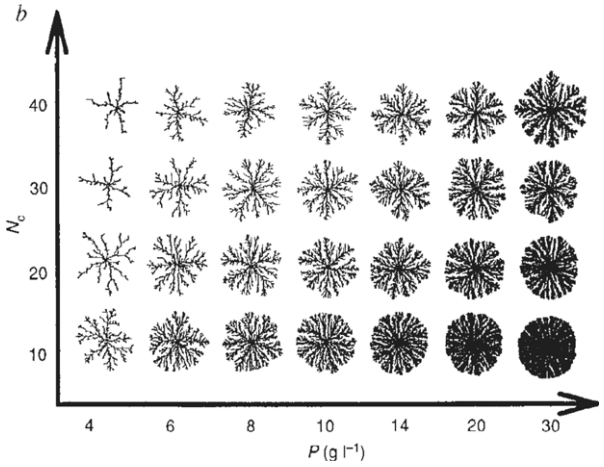

Fig. 5(a). Numerical simulation results of growth patterns as function of peptone level P (initial value of c) and N_c (agar concentration).

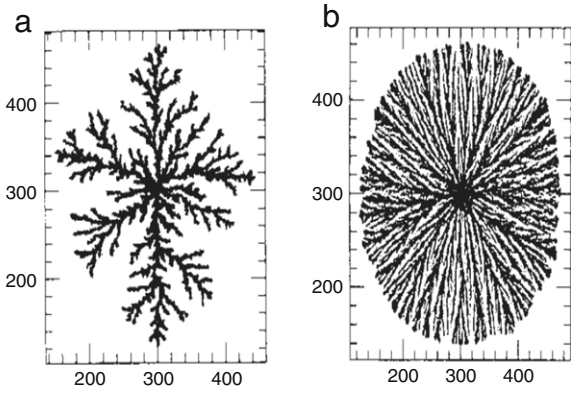

Fig. 5(b). Effect of chemotaxis on CA model with $P = 10\ \mathrm{gl}^{-1}$, $N_c = 40$. (a) No chemotaxis, (b) With chemotaxis.

of the global oxygen uptake rate, the concentration profiles for the oxygen, and biomass and colonies, size were both qualitatively and quantitatively in agreement with experimental data in [28–30].

[31] developed a three-dimensional multispecies biofilm model based on CA approach and tested it with a two-species biofilm composed of sulfate-reducing bacteria and methanogens. The model predicts different biofilm structures in the absence of sulfate, when a syntrophic association between the two organisms develops, and in the presence of sulfate, when the two organisms compete for the available hydrogen.

In [32], a 2D CA model was developed to study the effect of the thickness of the substrate's concentration and the hydrodynamic boundary layers in the biofilm's structure, motivated by the experimental results of [33,34]. The model predicts that when external mass transfer (for substrate) limitations are significant, the biofilm develops more open structures; when the substrate concentration layer is reduced and the external mass transfer is enhanced, the biofilm develops denser and smooth structures. The simulation reproduced the "mushroom" shaped biofilm described by [35].

A computer model called BacLAB based on the solute diffusion model coupled with the CA principles for the bacterial growth was developed by Hunt et al. [36,37] to study the detachment mechanisms in a biofilm. This computer model has been used to test various hypothetical detachment mechanisms in 3-D simulations [38,39]. These studies show that the detachment is a critical determinant of the biofilm's structures and of the dynamics of the biofilm's accumulation and loss.

For the models described in this section, the effect of the surrounding bulk fluid is not coupled explicitly. We next discuss models that couple the bulk fluid to the biofilm completely. More sophisticated models combining the CA and a continuous description of the bulk fluid will be described later.

5. Biofilms models with biomass and flow coupling

For most of the biofilm models described in previous sections, the biofilm's structure is primarily determined by the substrate concentration which is solely modeled by diffusion process. However, the heterogeneous structures including a nonuniform distribution of cells and polymers, variable biofilm thickness and surface shape, and variable density and porosity, have been observed and quantitatively measured by many researchers [40–42]. It is also found that the hydrodynamics of the bulk fluid plays an important role in shaping the structure of the biofilms through both the convection of the nutrient and the detachment of biomass by shear stress [43–45]. It is generally accepted that the formation of the biofilm's structure is the result of a combination of several simultaneously occurring biological, chemical and physical processes including cell transport to the substratum and attachment, the biofilm's generation by cellular growth and extracellular polymer production, the biofilm's detachment by shear stress, and substrate and product transport to and from the biofilm. Based on the previously established models and a better understanding of the biofilm's properties through experiment, several biofilm models coupling the bulk fluid were developed.

5.1. Hybrid discrete-continuum models

In [46–48], a fully quantitative two- and three-dimensional biofilm model was developed which incorporates the flow over the irregular biofilm's surfaces, convective and diffusive mass transfer of substrate, bacterial growth and biomass spreading. In this model, the biomass growth and spreading is modeled by the discrete CA model, the mass balance of the substrate is modeled by the continuity equation and the convection–diffusion–reaction equation, respectively, and the flow field is governed by the momentum balance (Navier–Stokes) equation. The fluid flow affects the biofilm's growth by both regulating the substrate concentration at the biofilm-fluid interface, shearing the biofilm's surface and eroding the protuberances. The interaction is reciprocal since a new biofilm's shape leads to a different boundary condition and thus different flow and substrate concentration.

The governing equations describing the biofilm model given in [46] are:

- Total mass conservation for fluid phase (the continuity equation):

$$\nabla \cdot \mathbf{u} = 0.$$

- Momentum conservation for the fluid phase flowing around the biofilm (the Navier-Stokes equation):

$$\frac{\partial \mathbf{u}}{\partial t} + \mathbf{u} \cdot \nabla \mathbf{u} = -\frac{1}{\rho}\nabla p + \nu \nabla^2 \mathbf{u}.$$

- Mass conservation for one dissolved substrate (for the limiting substrate only):

$$\frac{\partial C_S}{\partial t} + \mathbf{u} \cdot \nabla C_S = -R_S(C_S, C_X) + D\nabla^2 C_S.$$

- A kinetic equation for biomass growth:

$$\frac{\mathrm{d}C_X}{\mathrm{d}t} = R_X(C_S, C_X)$$

where **u** is the fluid velocity, p is the pressure, ρ is the liquid density, ν is the kinematic viscosity of the fluid, D is the substrate's diffusion coefficient, R_s and R_X are the rates of the substrate's consumption and biomass formation, C_S and C_X are the concentration of the substrate and biomass, respectively.

There is a clear separation of time scales in the biofilm's growth [47], namely, (1) the biomass growth and decay, in the order of hours or days, (2) the substrate transport, in the order of minutes, and (3) the hydrodynamic processes, in the order of seconds. Instead of solving all the equations in the smallest time-step given by the momentum equation, a process occurring at a particular time scale is solved while assuming all the other processes at different time scales are at steady state. For example, while solving the substrate mass-balance equation, the flow pattern is considered at a pseudoequilibrium for a given biofilm shape, and at the same time the biomass growth, decay, and detachment are in a frozen state. This leads to the following strategy in simulating the biofilm's development in time [46]:

1. Momentum transfer and continuity equations are solved to find the flow field variables: velocity **u**, pressure p, and the normal and tangential stresses τ acting on the biofilm's surface. This hydrodynamic step is needed each time the biofilm's geometry changes, either due to growth or detachment.
2. The flow velocity **u** calculated in the previous step (the flow is considered completely established) is used to solve the convection-diffusion-reaction equation for the mass conservation of the substrate. This equation is solved towards a pseudosteady-state substrate concentration, namely, $\frac{\partial C_S}{\partial t}$ is set to zero. In the first two steps, the equations were solved by a lattice Boltzmann algorithm [49–51]. In the absence of a convection term, a finite difference method was used to solve the substrate equation.
3. The new biomass content of each grid element, C_X, is calculated using the Monod and Herbert–Pirt equation including the substrate's concentration at a steady-state as calculated before.
4. As the biomass grows, it is redistributed in space according to the discrete CA rules used in [27]: by splitting the biomass content in the element in which it has grown above the maximum biomass density and by pushing the neighbors to reach the free space.
5. A detachment step can be performed before the redistribution. A traditional finite element method can be used to compute the deformation energy in the biofilm induced by the fluid stresses at the biofilm's surface, and places where the biofilm will break can be determined. The loss of biomass will cause a change of the external biofilm's structure so that a new hydrodynamic step is necessary.

One advantage of the discrete model of the biomass is that, once the model equations have been developed, the boundary conditions and the geometry of the system can be easily changed. For example, the carrier's surface can be spherical instead of flat, and it can be used to model the development of biofilms in particle reactors.

Numerical simulations in 2D and 3D were carried in [46]. The 3D model predicted that in a substrate limited regime the biofilm develops as a heterogeneous structure, presenting pores, channels and "mushroom"-like bacterial clusters, whereas in a substrate sufficient regime a compact, and densely-packed biofilm forms. The 2D models predicted that at high *Re* numbers, the thickness of the substrate concentration boundary layers (CBL) decreases and the biofilm develops a smooth surface; whereas at low *Re* numbers, the thickness of the CBL increases and yields a steep substrate concentration gradient, thus a rough biofilm with a finger-like shape forms.

A more detailed and quantitative study on the effect of diffusive and convective substrate transport on the biofilm's structure formation using this model was performed in [47] in a 2D case. The model's parameters characterizing the biofilm growth condition include: the growth ratio G, defined as $G =$ (maximum biomass growth rate)/(maximum internal transport rate of substrate), the Reynolds number *Re*, and the inoculation density s_0 (the percentage of substratum surface initially covered by the biofilm). Note that the large value of G corresponds to a substrate limited regime (high metabolic rate), and a small value of G corresponds to a substrate sufficient regime (low metabolic rate). A quantitative analysis of the simulated biofilm structure was achieved by calculating measures including the biofilm's area enlargement (α), the coefficient of surface roughness (σ), compactness (ξ), the porosity (ϵ) and the maximum biofilm's thickness (δ) as defined in [52]. The simulated biofilm's evolution in time is shown in Fig. 6 [47]. The model again predicts that under the limited substrate regime, biofilms develop an irregular surface with a high surface roughness, high surface area, high porosity, and low degree of compactness. As the substrate concentration increases, biofilms gradually shift to more compact and smooth structure. The model in this paper does not include the biofilm's detachment effect. It predicts that the effects of convection and of a flow-driven mechanism on the biofilm's structures are less important. It also predicts that a smaller inoculation density leads to a rougher biofilm, and the substrate flux to the biofilm is greatly influenced by both the internal and external mass transfer rates, but not by the inoculation density.

In [48], a two dimensional model was developed for the detachment based on the internal stress created by a moving fluid past the biofilm. This model used the strategy listed in this section with step 5 implemented, and it can model two biofilm detachment mechanisms, erosion (small-particle loss) and sloughing (large-biomass-particle removal) in a unified way. The model predicts that erosion makes the biofilm surface smooth and sloughing leads to an increased biofilm-surface roughness. Simulations also indicated an avalanche effect in the biomass's loss, and fast growing biofilms have a faster detachment rate than slow-growing biofilms, and thus suffers an instability in the biofilm's accumulation and an abrupt biomass loss.

The hybrid discrete-continuum biofilm model was a fully quantitative model incorporating many physical, chemical and biological processes affecting the biofilm's development. The quantitative nature of the model not only produced simulation results in good agreement with experimental data, but also predicted the properties of biofilms and shed light on experimental studies. The model was widely accepted and successfully applied to several situations since its development.

Another completely different discrete-continuum biofilm model was proposed by [53,54] based on the Immersed Boundary Method. In this microscale model, the microbes in the biofilm are treated as discrete entities (cells) which can swim through the action of flagellae, the bulk fluid is treated as a continuum, and the formation of the biofilm is achieved by a cell-cell aggregation and a cell-substratum adhesion which are modeled by generating the appropriate binding forces between discrete representations of the organisms. The model includes the hydrodynamic interaction between the biofilm and the fluid, the substrate reaction, diffusion and convection, and the chemotactic responses of swimming microbes. Numerical simulations in 2D predicted that the higher local cohesion forces and cell motility can greatly facilitate the biofilm's formation, cells may adhere preferentially to a saturated surface with chemotaxis, and changes of the channel's geometry also have effects on the surface irregularities in the biofilm's formation.

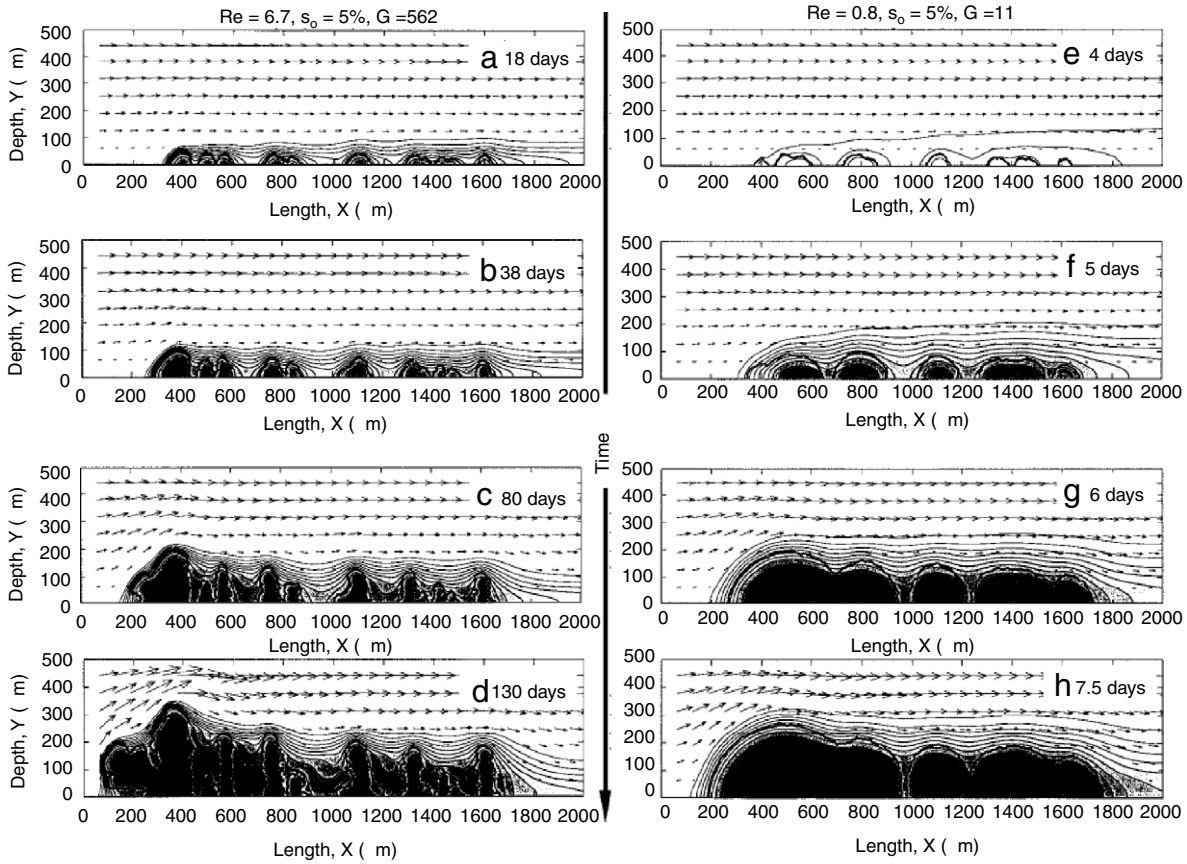

Fig. 6. Simulated biofilm evolution in time for (a–d) $Re = 6.7$, $s_0 = 5\%$, $G = 562$ and (e–h) $Re = 0.8$, $s_0 = 5\%$, $G = 11$. The arrows represent the vector velocity at intervals of 16 grid nodes. The thick lines indicate the biofilm's surface. Iso-concentration lines show the decrease of the substrate's concentration from the maximum value in the bulk liquid (white patches) to zero in the biofilm (dark gray patches), with a variation of 10% between the lines.

5.2. Multidimensional continuum models

The hybrid discrete-continuum models of multiple steps described previously (CA models) can produce results in good agreement with experimental expectations. However, there are some drawbacks associated with the element of randomness in the step of the biomass redistribution. Namely, they are lattice dependent and not invariant to changes of the coordinate system; multiple simulations with the same initial condition generally produce different outputs; the biomass, though a continuous variable according to the growth kinetics, suffers discrete changes during splitting. This randomness can be viewed as an artifact from the detail of the algorithm rather than the growth process modeled. Even though the random feature of these models determines the biofilm's structure to some extent, sometimes a deterministic model is more desirable. Several deterministic continuum biofilm models were developed to accommodate the need.

[55] developed a spatio-temporal continuum model under which the biomass spreading is described by a nonlinear density-dependent diffusion mechanism. The whole region is divided into a bulk liquid region Ω_1 without biomass and a solid biofilm region Ω_2 where all the biomass is contained. The governing system of equations is given by:

$$\nabla \cdot u = 0,$$
$$\frac{\partial u}{\partial t} + u \cdot \nabla u = -\frac{1}{\rho}\nabla p + \nabla^2 u, \quad \text{in } \Omega_1 = \{x \in \Omega \mid m(t,x) = 0\},$$
$$u \equiv 0, \quad \text{in } \Omega_2 = \{x \in \Omega \mid m(t,x) > 0\},$$
$$\frac{\partial c}{\partial t} + u \cdot \nabla c = \nabla \cdot (d_1(m)\nabla c) - f(c,m),$$
$$\frac{\partial m}{\partial t} = \nabla \cdot (d_2(m)\nabla m) + g(c,m),$$
$$f(c,m) = \frac{k_1\, cm}{k_2 + c} \qquad g(c,m) = k_3(f(c,m) - k_4 m).$$

Here $u(t,x)$ is the fluid velocity, $p(t,x)$ is the fluid pressure, $m(t,x)$ is the biomass density, $c(t,x)$ is the nutrient concentration, $d_{1,2}$ are diffusion coefficients for c and m, $f(c,m)$ is the nutrient consumption rate, $g(c,m)$ is the biomass production rate, and $k_1, \ldots, k_4$ are constants. In this paper, $d_1(m)$ is considered a constant and the density-dependent diffusion coefficient $d_2(m)$ is given by

$$d_2(m) = \left(\frac{\epsilon}{m_{\max} - m}\right)^a \cdot m^b.$$

Thus the diffusion operator in the equation for $m(t,x)$ degenerates for a small biomass and is singular at the biomass density bound $m_{\max}$. The parameters a, b, ϵ are chosen to guarantee the following properties: 1. there exists a "sharp interface" between the biomass and the bulk fluid, 2. biomass spreading is significant only if a certain maximum density is approached, 3. biomass density cannot exceed the maximum bound $m_{\max}$. Simulations under a hydrostatic condition ($u \equiv 0$) were conducted in 1D and 3D, which yield the following observations. Biofilms develop a spatial heterogeneous structure under a heterogeneous environment (either nutrient concentration or inoculation density). With limited nutrients, the biofilm tends to develop isolated colonies with channels in between, thus a rough structure. With a sufficient amount of nutrient, the biofilm tends to develop a more compact structure with colonies connected to each other. In either case, mushroom-shaped colonies dominating over their smaller neighbors were observed, which is in good agreement with experiments (*e.g.* [1]).

[56] developed a continuum model of a single substrate limited biofilm growing into a static aqueous environment. The region under consideration in $\mathbb{R}^3$ is divided into a biofilm region $z \leq h(x, y, t)$ and an aqueous region $z > h(x, y, t)$, with the interface $z = h(x, y, t)$. The biofilm is modeled as a homogeneous, viscous, incompressible fluid with a velocity $\mathbf{u}$ given by Darcy's law

$$\mathbf{u} = -\lambda \nabla p$$

where p is the pressure and λ is a constant. Despite the incompressibility, the growth (or decay) of the biofilm yields a field of sources (or sinks) in the biofilm fluid. Thus

$$\nabla \cdot \mathbf{u} = g$$

for some prescribed growth function g. Combining these two equations yields

$$-\lambda \nabla^2 p = g.$$

The normal velocity of the biofilm's interface $(x, y, h(x, y, t))$ is $\mathbf{n} \cdot \mathbf{u}|_{z=h^-} = -\mathbf{n} \cdot \lambda \nabla p|_{z=h^-}$, where $\mathbf{n}$ is the unit upward normal and h^- means that z should approach h from below, the biofilm side. Since p is proportional is λ^{-1}, the interface velocity is independent of λ. This is true since the velocity $\mathbf{u}$ is generated by the biofilm's growth, and thus depends only on g but not on λ. The aqueous region $z > h$ is assumed to be static. Hence the boundary conditions for p are given by $p|_{z=h} = 0$ and $p_z|_{z=-\infty} = 0$, where $z = -\infty$ corresponds to the bottom of the domain. The concentration of a single limiting substrate is denoted by $S(x, y, z, t)$. Substrate diffuses through the aqueous region into the biofilm, where it is consumed and diffuses with a different diffusion coefficient. It is assumed that there is a function $H(x, y, z, t)$ with $H \geq h$ such that $S(x, y, z, t) = S_\infty$ for $z \geq H$. The substrate's equations are

$$S_t - D_1 \nabla^2 S = 0, \quad h < z < H,$$
$$S_t - D_2 \nabla^2 S = -u(S), \quad z < h,$$

with boundary conditions $S|_{z=H} = S_\infty, S_z|_{z=-\infty} = 0$, and matching conditions $S|_{z=h^+} = S|_{z=h^-}, D_1 \nabla S|_{z=h^+} = D_2 \nabla S|_{z=h^-}$. The substrate uptake rate $u(S)$ is defined by the Monod function

$$u(S) = u_{\max} \frac{S}{S + K_S},$$

and the growth function $g(S)$ is taken as a function of $u(S)$, namely, $g = g(u(S))$. The equations are nondimensionalized by introducing a characteristic time scale T and length scale w. Since the substrate diffusion occurs much faster than the biofilm's growth, it is assumed to be in a steady state and S_t is set to zero in the equation. The dimensionless equations of the model are given by

$$\nabla^2 p = -g(u(S)), \quad z < h,$$
$$-\nabla^2 S = 0, \quad h < z < H,$$
$$-\nabla^2 S = -Gu(S), \quad z < h,$$

with boundary conditions described above. Here $G = w^2 u(S_\infty)/D_2$ S_∞ is the nondimensional growth number. One dimensional moving front solutions are analyzed by writing the equation for S as a first order system of ODEs, and analytical solutions are presented for the particular choices of u and g. It shows that the penetration depth of the substrate into the biofilm is $O(G^{-1/2})$. Linear stability analysis shows that if the substrate concentration S is sufficient low, the planar front solutions suffer a fingering instability with preferred wavelength of the order of $O(G^{-1/2})$. Nonlinear evolution of the finger instability in 2D is studied through numerical simulations, where the level set method is used to track the interface $z = h$. This continuum model provides scaling predictions of the biofilm's growth process and can be compared to experimental data, and it is among the early work of the rigorous mathematical treatment of biofilm models.

[57] extended the work in [56] and proposed a multidimensional continuum model for the heterogeneous growth of biofilm systems with multiple species and multiple substrates while retaining Darcy's law for the velocity. The model was tested for two systems. System 1 is the biofilm consisting of an active and inert biomass with oxygen as a substrate; system 2 is the biofilm consisting of heterotrophs, autotrophs, and inerts with limiting substrates of oxygen, acetate, and ammonium. Numerical simulations were performed in 2D and 3D. It predicted that for system 1, the inactivation rate has an effect on the stability of the biofilm's interface, namely, a higher inactivation rate increases the depth of the active layer by locally decreasing the amount of active biomass. For system 2, the 2D simulation produced results in agreement with [9]; but the 3D simulation yielded the total averaged mass fractions of the biofilm components not adding to 1 due to the heterogeneity of the biofilm surface, a multidimensional phenomenon cannot be described by the 1D model in [9].

[58] proposed a continuum model in which the biofilm is treated as a biological gel composed of an extra-cellular polymeric substance (EPS) and water. The bacteria are enmeshed in the network and are the producers of the polymer. Gels absorb or expel solvent causing a swelling or contraction due to the osmotic pressure gradients, where the physical and chemical environmental conditions affecting the biofilm morphology are built into the osmotic pressure. The model assumes that the primary forces which induce the gel's motion are applied to the fluid solvent and the EPS, and provide a mechanism of biomass redistribution through swelling of the EPS and the constitutive relationships. Here both the network and the solvent are treated as Newtonian fluids with a much larger viscosity for the network. This fundamental formulation of the model follows the two-fluid model [59]. However, the inertia is neglected so that the governing equation for the force balance is the Stokes equation for multi-fluids.

The volumes of the substrate and the bacteria are assumed to be negligible and the volume fractions of the polymer network and solvent are denoted by θ_n and θ_s respectively. Four forces acting on the network are assumed, including the viscous stress $\nabla \cdot (\theta_n \sigma_n)$, the frictional drag between the network and the solvent, the gradient of an osmotic pressure $\nabla \Psi(\theta_n)$ representing the force induced by the colligative properties of the gel, and the hydrostatic pressure. The forces acting on the solvent include all the forces described above except the osmotic pressure. Here σ_n is the viscous stress tensor given by $\sigma_n = \frac{\eta_n}{2}(\nabla \vec{U}_n + \vec{U}_n^T)$, $\vec{U}_n$ is the network's velocity and η_n is the network's viscosity. The osmotic pressure $\Psi(\theta_n)$ is obtained by a Taylor's expansion of the Flory–Huggins formula up to θ_n^3 around $\theta_n = 0$, and the expression is

$$\Psi(\theta_n) = \frac{k_B T}{3 v_1} \theta_n^2 \left(\theta_n - 3 \left(\chi_1 - \frac{1}{2} \right) \right).$$

Here k_B is the Boltzmann's constant, T is the temperature, v_1 is the volume of one monomer of the network constituent, and χ_1 is the Flory–Huggins interaction parameter. The analysis is done for a simplified model obtained by ignoring the inertial term, setting the frictional force to zero and assuming a zero solvent velocity, which in turn yields a zero hydrostatic pressure gradient. Thus the simplified network's momentum equation is

$$\nabla \cdot (\theta_n \sigma_n) - \nabla \Psi(\theta_n) = \eta_n \nabla \cdot \left(\frac{\theta_n}{2} \left(\nabla \vec{U}_n + \nabla \vec{U}_n^T \right) \right) - \nabla \Psi(\theta_n) = 0. \tag{5.1}$$

The network's redistribution is governed by the principle of conservation of mass, and the governing equation is

$$\frac{\partial \theta_n}{\partial t} + \nabla \cdot (\theta_n \vec{U}_n) = g_n. \tag{5.2}$$

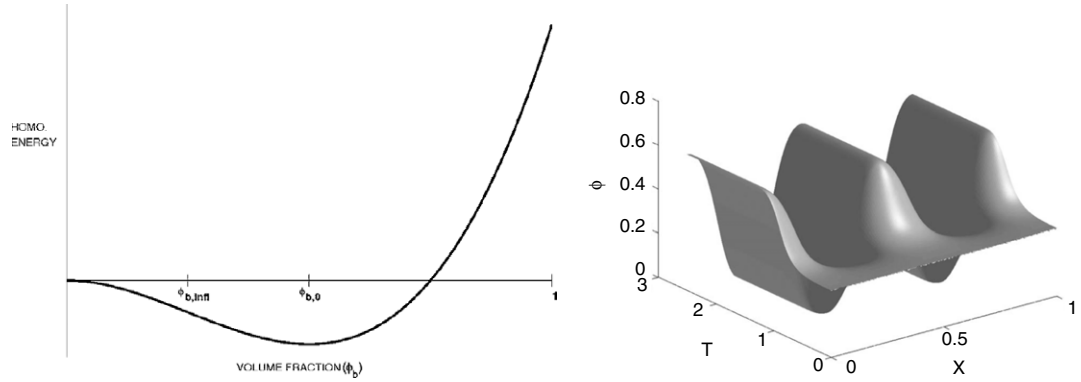

(a) Mixing energy density $f(\phi_b)$.

(b) Solution starting with a random perturbation of the constant solution.

Fig. 7. Cohesion energy model.

The substrate concentration c is governed by the following convection-diffusion-reaction equation:

$$\frac{\partial(\theta_s c)}{\partial t} + \nabla\cdot(c\vec{U}_s\theta_s - D\theta_s\nabla c) = -g_c.$$

Here $\vec{U}_s$ is the solvent velocity and the scaling factor θ_s reflects the fact that the substrate is dissolved in the solvent. Since $\theta_s = 1-\theta_n$, $\vec{U}_s = 0$, the substrate is assumed to be in quasi-steady-state, and the consumption rate is taken as $g_c = A\theta_n c$, the substrate equation becomes

$$D\nabla\cdot((1-\theta_n)\nabla c) = A\theta_n c. \tag{5.3}$$

The growth of the EPS network is modeled by Monod kinetics, i.e., $g_n = \epsilon\mu\theta_n\frac{c}{K_c+c}$, where K_c is the half-saturation constant and μ is the maximum production rate. In the substrate limited regime ($c \ll K_c$), g_n can be approximated by $g_n = \epsilon A\theta_n c$, where $A = \frac{\mu}{K_c}$. The system of the governing equations of the model are given by (5.1)–(5.3), and the variables are θ_n, $\vec{U}_n$, c. The interface between the biofilm region ($\theta_n > 0$) and the solvent region ($\theta_n = 0$) is not explicitly tracked, but is characterized by a rapid change in θ_n. Linear stability analysis of the flat interface shows that there is a maximally unstable mode and the higher frequency perturbations are damped out, which is in qualitative agreement with the result of [56]. Numerical simulations were performed in 2D. This model lays out the framework of studying the effect of the material and the chemical properties (network viscosity, osmotic pressure) on the biomass's distribution, and produces results in qualitative agreement with previously developed models. The idea of using the network volume fraction θ_n to represent the biofilm provides the possibility of modeling the whole biofilm system as a multi-phase fluid.

Experimental results in [60] indicate that the detachment of multicellular clumps is more significant than the erosion of single cells, possibly because clumps retain certain advantages of the biofilm. [61] proposed a more general multi-fluid model to explain this phenomenon by the cohesion energy. Let ϕ_b and ϕ_s be the volume fractions of the biomaterial and the solvent with $\phi_b+\phi_s = 1$, $\mathbf{u}_b$ and $\mathbf{u}_s$ being the velocities of the biomaterial and solvent, and the whole system is incompressible so the volume average velocity $\mathbf{u} = \phi_b\mathbf{u}_b + \phi_s\mathbf{u}_s$ is divergence free. A cohesive energy $E(\phi_b)$ of the form

$$E(\phi_b) = \int\left(f(\phi_b) + \frac{\kappa}{2}|\nabla\phi_b|^2\right)\mathrm{d}V$$

is introduced. Here $f(\phi_b)$ is the mixing energy density (Fig. 7(a)) with a minimum at $\phi_{b,0}$ and an inflection point at $\phi_{b,infl}$. The term $\frac{\kappa}{2}|\nabla\phi_b|^2$ penalizes the rough change of ϕ_b at small-scales. Using $(\mathrm{d}/\mathrm{d}t)\phi_b + \nabla\cdot(\phi_b\mathbf{u}_b) = 0$ (the mass conservation of ϕ_b with growth term neglected), the time derivative of E is calculated as

$$\frac{\mathrm{d}E}{\mathrm{d}t} = -\int(\phi_b\nabla\cdot\Pi)\cdot\mathbf{u_b}\mathrm{d}V \tag{5.4}$$

where

$$\Pi = -[f'(\phi_b) - \kappa\nabla^2\phi_b]I$$

is a cohesive stress tensor. Eq. (5.4) is in the form of a work integral $\dot{E} = \int\mathbf{f}\cdot\mathbf{u}_b\mathrm{d}V$, hence the force term $\phi_b\nabla\cdot\Pi$ must be included in the momentum balance equation for the biomaterial. Neglecting the inertial and viscous and viscoelastic stresses terms, the momentum equations for ϕ_b and ϕ_s are

$$0 = \phi_b\nabla\cdot\Pi - \zeta(\mathbf{u}_b - \mathbf{u}_s) + \phi_b\nabla p$$
$$0 = -\zeta(\mathbf{u}_s - \mathbf{u}_b) + \phi_s\nabla p$$

where p is the hydrostatic pressure and $\zeta(\mathbf{u}_b - \mathbf{u}_s)$ is the frictional coupling between biomaterial and solvent with $\zeta = \zeta_0\phi_b\phi_s$. Some algebraic manipulations yield an equation for ϕ_b as

$$\frac{\partial\phi_b}{\partial t} + \nabla\cdot(\phi_b\mathbf{u}) = \nabla\cdot[a(\phi_b)f''(\phi_b)\nabla\phi_b] - \kappa\nabla\cdot[a(\phi_b)\nabla\nabla^2\phi_b]$$

where $a(\phi_b) = \zeta_0^{-1}\phi_b(1-\phi_b)$. Analysis and a numerical simulation were performed in the 1D case, where the boundary conditions and the incompressibility yield $\mathbf{u} = 0$ and the equation for ϕ_b becomes a modified Cahn–Hilliard equation. The model predicted that a minimization of the cohesive energy results in a spontaneous formation of free surface films. Furthermore, in the presence of the cohesion energy for a sufficiently low density biomaterial, the one-dimensional system appears to spontaneously separate into microcolonies due to a spinodal decomposition instability (Fig. 7). This model suggests that the cohesion energy is fundamental to many aspects of the biofilm's mechanics. We remark that this mode and the model proposed by Keener and Cogan are essentially the same. They only differ in minor details, both of which belong to the class of binary or two fluid models.

Experiments [43,62] also indicate that the biofilm responds elastically to a mechanical stress on short time scales and behaves as a viscous fluid on long time scales. Early work of modeling biofilm as a viscoelastic fluid includes [63]. Researchers are now starting to build biofilm models using more sophisticated constitutive equations to capture the viscoelastic nature of the biofilm.

Most of the models described above either track the biofilm–fluid interface explicitly [46–48,56], or assume that the solvent has zero velocity [55,58]. Motivated by the work from [56,58,61] and other researchers, but in particular frustrated by the lack

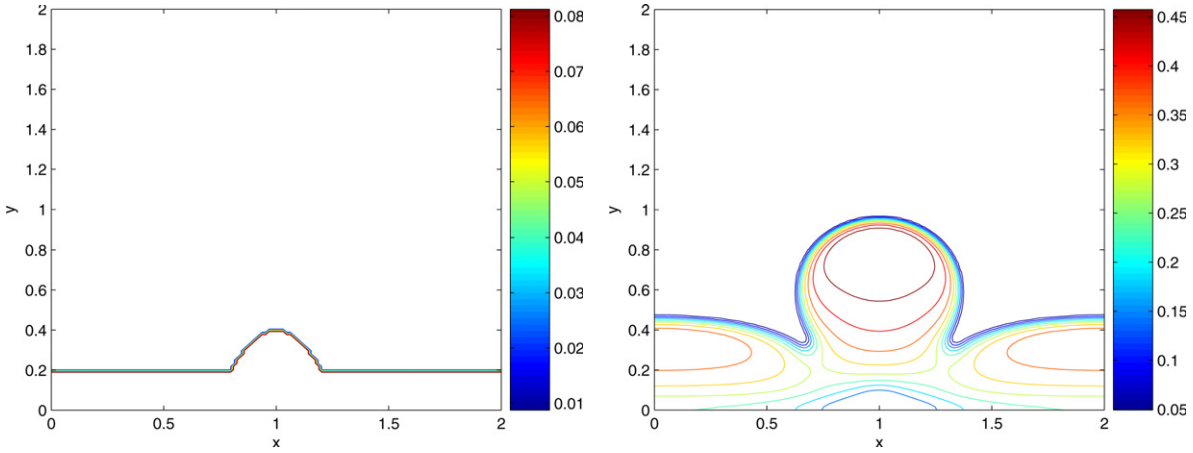

(a) $t = 0$. (b) $t = 300$.

Fig. 8. Growth of mushroom shaped biofilm.

of mathematical machinery to handle the inlet and outlet boundary conditions in the multi fluid models, [64,65] proposed a phase-field biofilm model. The model is based on the one-fluid two-component formulation in which the combination of the extracellular polymeric substances (EPS) and the bacteria is effectively modeled as one fluid component, while the collective ensemble of the substrate and the solvent are modeled as the other. The biofilm is assumed to be an incompressible continuum, in which the relative motion of the polymer network and the solvent relative to the average velocity is accounted for by mixing kinetics. This model can be shown to be a closure model of a more general kinetic theory for biofilm mixtures [66].

Let $\mathbf{v}$ be the average velocity, p the pressure, ϕ_n and ϕ_s the volume fraction of the polymer network and the solvent respectively, and c the substrate concentration, the phase field model for biofilms (treated as viscous fluids) consists of the following four equations in dimensionless form:

$$\nabla \cdot (\mathbf{v}) = 0,$$

$$\rho \frac{\mathrm{d}\mathbf{v}}{\mathrm{d}t} = \nabla \cdot (\phi_n \tau_n + \phi_s \tau_s) - [\nabla p + \Gamma_1 \nabla \cdot (\nabla \phi_n \nabla \phi_n)],$$

$$\frac{\partial}{\partial t}(\phi_s c) + \nabla \cdot (c\mathbf{v}\phi_s - D_s \phi_s \nabla c) = -g_c,$$

$$\frac{\partial \phi_n}{\partial t} + \nabla \cdot (\phi_n \mathbf{v}) = \nabla \cdot \left(\Lambda \phi_n \nabla \frac{\delta f}{\delta \phi_n} \right) + g_n$$

where

$$\tau_n = \frac{2}{Re_n}\mathbf{D}, \qquad \tau_s = \frac{2}{Re_s}\mathbf{D}, \qquad \mathbf{D} = \frac{\nabla \mathbf{v} + \nabla \mathbf{v}^T}{2},$$

$$g_c = A\phi_n \frac{c}{K_n}, \qquad g_n = \epsilon \mu \phi_n \frac{c}{K_c + c}.$$

The mixing free energy density is given by

$$f = \frac{\Gamma_1}{2} \|\nabla \phi_n\|^2 + \Gamma_2 \times \left[\frac{\phi_n}{N} \ln \phi_n + (1 - \phi_n) \ln(1 - \phi_n) + \chi \phi_n (1 - \phi_n) \right].$$

Here we consider that the network and the solvent have the same density ρ, Re_n and Re_s are the Reynolds numbers of the network and the solvent respectively, D_s is the diffusion coefficient for the substrate, and Λ, Γ_1, Γ_2 are dimensionless constants associated with the mobility, strength of the distortional free energy and that of the bulk energy. Here f is an extended Flury–Huggins free energy density including the distortional free energy term $\frac{\Gamma_1}{2} \|\nabla \phi_n\|^2$, which accounts for the surface tension effect at the biofilm–solvent interface defined by $\phi_n = 0$, N is the generalized polymerization index, and χ is the Flory–Huggins mixing parameter. Steady state solutions are identified, and the linear stability analysis shows that the flat biofilm–solvent interface is unstable for a finite interval of perturbation modes, with a single maximally unstable mode, which is in agreement with [56,58]. Numerical simulations in 2D captured various phenomena observed in experiments including a mushroom shaped growth (Fig. 8), detachment due to shear stress of the flow (Fig. 9), rippling and erosion, etc. The advantage of modeling biofilms as a multicomponent material includes the robust treatment of the physics and the interacting dynamics among the components. Meanwhile, deriving a model consisting of a single fluid eliminates several difficulties associated with the coupled biofilm-bulk fluid flow such as velocity, boundary conditions, etc. In particular, the interface conditions are dramatically simplified, since the interface is not separated from the rest of the system. In addition, influent and effluent boundary conditions are natural in the single fluid case. It also provides a framework in which various constitutive relations for each constituent can be investigated in conjunction with the motion of the bulk fluid. The model presented above is the viscous limit of a more general viscoelastic model which we will discuss later.

6. Individual-based Modeling (IbM)

[67,68] proposed the Individual-based Modeling (IbM) of biofilms. The model consists of two parts: one deals with the the growth and behavior of individual bacteria as autonomous agents; the other deals with the substrate and product diffusion and reaction (Fig. 10(a)). Bacterial cells are represented as hard spheres, with each cell having, besides a variable volume and mass, a set of variable growth parameters. Each cell grows by consuming the substrate and divides when a certain volume is reached. The pressure buildup due to the growth of biomass is released by maintenance of a minimum distance between the neighboring cells. For each cell, the vector sum of all positive overlap radii with the neighboring cells is calculated and then the position of the cell is shifted in the direction opposite to this vector. The substrate concentration is governed by a reaction-diffusion equation, thus IbM is a hybrid discrete-continuous model. The biomass spreading mechanism in IbM allows cell movement with a continuous distance and direction, which makes it a deterministic model and overcomes the drawbacks associated with the randomness in the CA based models. Fig. 10(b) shows

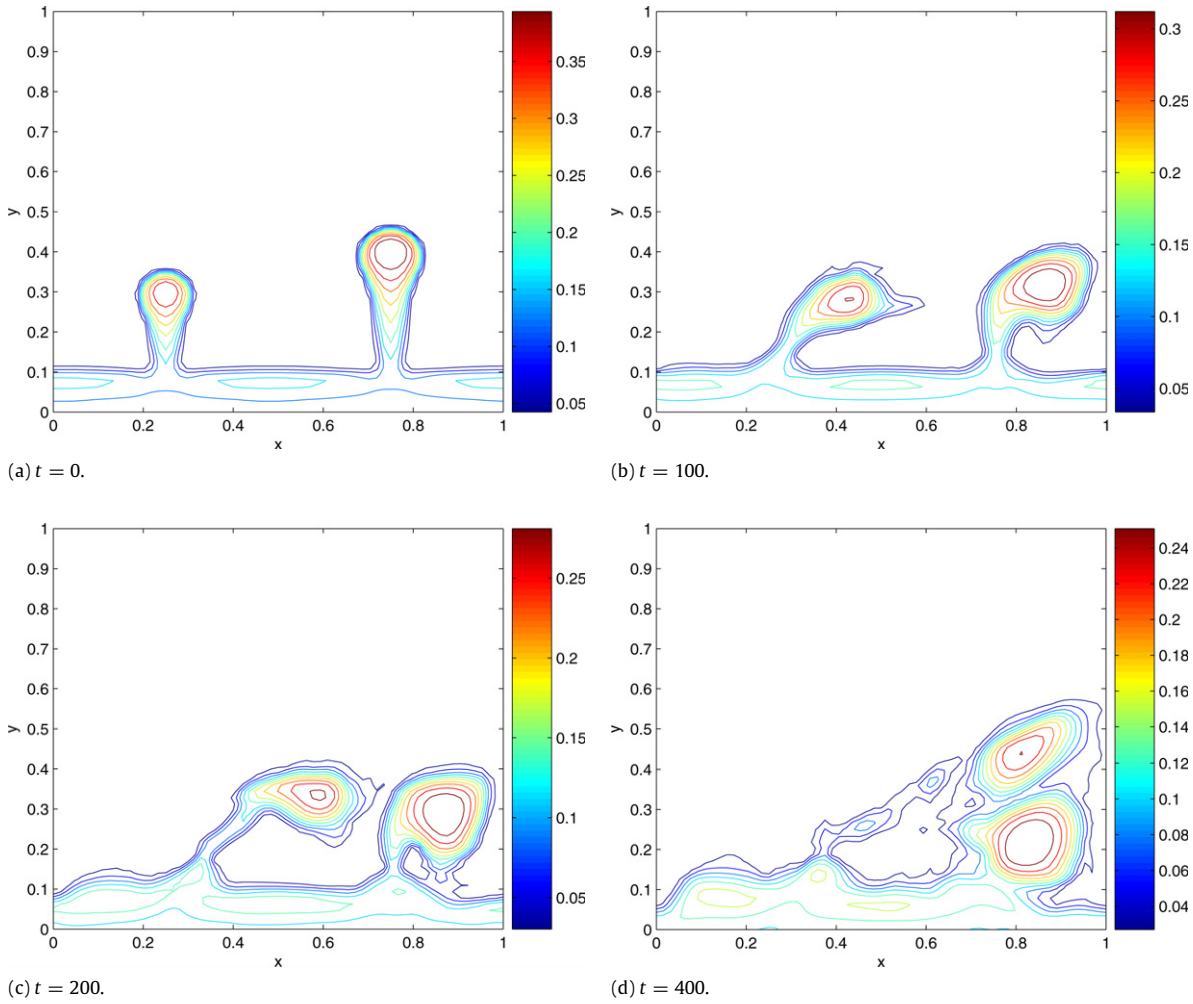

(a) $t = 0$. (b) $t = 100$.

(c) $t = 200$. (d) $t = 400$.

Fig. 9. Detachment induced by shear flow over two mushroom shaped biofilm.

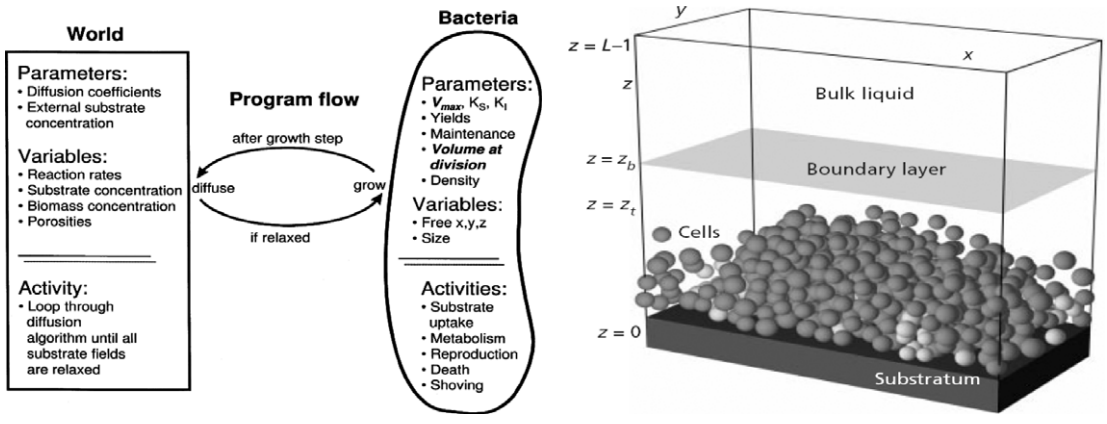

(a) Model structure. (b) Geometry.

Fig. 10. IbM model structure and schematic system geometry.

the computation domain of the model. Numerical simulations in 2D showed that the IbM model produced a more confluent and rounded biofilm structure than the CA based models, due to its deterministic and directionally unconstrained spreading of the biomass. [69] extended the IbM model and proposed a Particle-Based Multidimensional Multispecies Biofilm Model. This model allows variable size biomass particles in order to model the systems with a large-scale heterogeneity. Numerical simulations predicted that if only the average flux of nutrients needs to be known, the 2D and 1D models are very similar. However, the behavior of intermediates, which are produced and consumed in different locations within the biofilm, is better described in the 2D and 3D models because of the multidirectional concentration gradients. The predictions of the 2D or 3D models are also different from those of 1D models for slowly growing or minority species in the biofilm (see Fig. 10).

7. Other models related to the biofilm's properties

Most of the models described above concentrate on the biofilm's structure resulted from biomass growth and spreading, substrate transport and consumption. Experimental results also indicate that the biofilm exhibits complicated physical, chemical and biological properties during the interactions with the surrounding environment such as the external fluid flow and the antimicrobial agents. There are extensive studies on these biofilm properties and many models associated with that, and we will described a few of them in this section.

7.1. Antimicrobial penetration barrier

Bacterial cells inside the biofilm generally have a higher tolerance to chemical attack from antimicrobial agents compared to planktonic cells [70–72], and a widely accepted explanation is that the biofilm matrix acts as a protective barrier against attack. [73–75] proposed a theoretical framework to explain this phenomenon based on diffusion processes in biofilms. In this model, the biofilm is assumed to be a uniformly thick planar slab of thickness L_f with one side adjoining an impermeable boundary and the other side exposed to the bulk fluid. Fick's law of diffusion is used and the mass transfer resistance between the biofilm-fluid interface and the bulk fluid is neglected. The biofilm contains cells (volume fraction ϵ_c), extracellular polysaccharide (volume fraction ϵ_p), and water (volume fraction $\epsilon_w = 1-\epsilon_c-\epsilon_p$). The antimicrobial is modeled as a solute in the biofilm with a concentration C, and the spatial variable is z. Five cases were considered based on different properties of the solute in which the governing equations are given as follows:

1. Diffusion of a noninteracting solute.

$$\epsilon_w \frac{\partial C}{\partial t} = D_e \frac{\partial^2 C}{\partial z^2}.$$

2. Diffusion of a reversibly sorbing, nonreacting solute.

$$[\epsilon_w + (1-\epsilon_w)\kappa]\frac{\partial C}{\partial t} = D_e \frac{\partial^2 C}{\partial z^2}.$$

Here κ is a partition coefficient quantifying the equilibrium distribution of solute between the aqueous and biofilm phases.

3. Diffusion of an irreversibly sorbing, non-reacting solute

$$\epsilon_w \frac{\partial C}{\partial t} = D_e \frac{\partial^2 C}{\partial z^2} - k_s C X_s$$
$$\frac{\partial X_s}{\partial t} = -\frac{k_s C X_s}{Y_{cx}}$$
$$X_s(0,z) = X_s^0 \quad \text{for } 0 \le z \le L_f.$$

Here X_s is the concentration of free binding sites, k_s is the rate coefficient for the sorption process, Y_{cx} is a yield coefficient describing the mass of solute sorbed per mass of biofilm in which binding sites have been saturated.

4. Diffusion of stoichiometrically reacting solute. The governing equation is identical to the one in the previous case of irreversible sorption. Here Y_{cx} is the mass of solute neutralized per mass of biofilm reacted, and the sorption rate coefficient k_s is replaced with the reaction rate coefficient k_r.

5. Diffusion of a catalytically reacting solute

$$\epsilon_w \frac{\partial C}{\partial t} = D_e \frac{\partial^2 C}{\partial z^2} - k_r C.$$

In all the cases described above, C satisfied the same initial and boundary conditions given by

$$C(0,z) = 0, \quad \text{for } 0 \le z \le L_f$$
$$\left.\frac{\partial C(t,z)}{\partial z}\right|_{z=0} = 0, \qquad C(t,L_f) = C_0.$$

The parameter D_e is the effective diffusion coefficient in the biofilm, and it is expected to be smaller than the diffusion coefficient of water D_{aq}. Here D_e is determined by the following empirical formula

$$\frac{D_e}{D_{aq}} = \left(\frac{1-\epsilon_c}{1+\epsilon_c/2}\right)\left(\frac{(1-\epsilon_p^*)^3}{(1+\epsilon_p^*)^2}\right)$$

where $\epsilon_p^* = \epsilon_p/(1-\epsilon_c)$ is the polymer volume fraction in the intercellular space. Numerical simulations of the model predicted the following properties. A noninteracting solute was predicted to penetrate the biofilms of up to 1 mm relatively quickly, within seconds or minutes. In this case the solute does not sorb or react in the biofilm, therefore, the diffusion barrier is not large enough to account for the reduced susceptibility of biofilms to antibiotics. Reversible and irreversible sorption retards the antibiotic penetration. A catalytic reaction, provided it is sufficiently rapid, can lead to severe antibiotic penetration failure. This model provides guidelines for the design and analysis of experiments to test the mechanisms of reduced biofilm susceptibility to antibiotics.

7.2. Persisters

Besides the penetration barrier described above, another important hypotheses concerning the resistance mechanism to antimicrobial for the bacterial biofilms is the existence of "persister" cells which are extremely tolerant of the antimicrobials. Experimental results [76,77] demonstrate the existence of the persisters and indicate that the persisters are not genetic variants nor cells in a spore-like state nor cells caught coincidentally in a quiescent phase of cell division. A biofilm with persisters typically exhibits the bi-phasic disinfection curve, namely, the bacteria population versus disinfection time is of the form $p(t) = C_1\exp(-k_1 t) + C_2\exp(-k_2 t)$ with $k_1 > k_2$ and $C_1 \gg C_2$. Two different types of persister model will be described here.

[78] proposed a phenotype-switching model. The bacterial phenotypes are denoted by B_S and B_P for the susceptible and the persister cell density, and there is one growth-limiting substrate, denoted by S, and one antimicrobial, denoted by A. The population of the susceptible cells changes due to growth, death due to antibiotic action, loss due to transition to persister cells and gain as the persistent cells revert back to the susceptible cells. The governing equation of B_s is given by

$$\frac{dB_S}{dt} = \frac{\mu_{\max}}{Y}\frac{S}{K_S+S}B_S - k_d(A,t)\mu_{\max}\frac{S+\alpha}{K_s+S}B_S - k_l(A,t)\mu_{\max}\frac{S}{K_S+S}B_S + k_g(A,t)B_P.$$

Here the parameters k_d, α, k_l, k_g are assumed to be linearly proportional to A and the proportional constants are chosen to fit data from [77]. Persister's cells are not killed by the antibiotic, and the population changes are only due to cells converting to and from the susceptible cells. The equation for B_P is

$$\frac{dB_P}{dt} = k_l(A,t)\mu_{\max}\frac{S}{K_S+S}B_S - k_g(A,t)B_P.$$

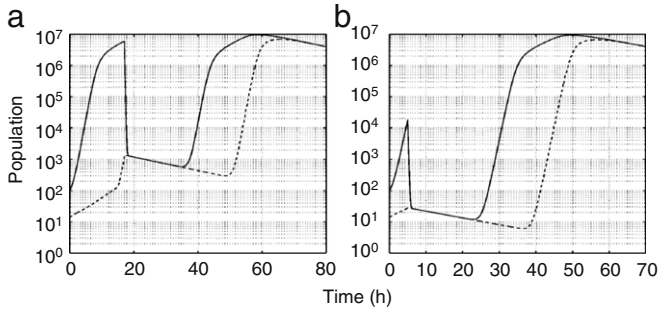

Fig. 11. Exposure of a batch culture to an antimicrobial. (a) Antimicrobial applied during the stationary phase at $t = 17$ h and removed at $t = 27$ h, at which time the surviving cells are recultured at the $t = 0$ h nutrient level. (b) Antimicrobial applied during the exponential phase at $t = 5$ h and removed at $t = 15$ h, at which time the surviving cells are recultured at the $t = 0$ h nutrient level. Solid lines, all cells; dashed lines, persisters.

The substrate is consumed only by the susceptible cells and the equation for S is

$$\frac{\mathrm{d}S}{\mathrm{d}t} = -\mu_{\max}\frac{S}{K_S + S}B_S.$$

Numerical simulation and analysis of a simplified model indicate that the relative dose/withdrawal times are important in determining the effectiveness of a periodic dosing treatment, and there is an optimal withdrawal length specific to the bacterial kinetics.

[79] proposed a model which treats the persister cells as senescent cells based on the idea that the senescent cells are slow-growing, and slow-growing cells are more tolerant to antimicrobials. Let $b(a, t)$ denote the bacterial population density at time t of the senescence level a. The governing equation of b is

$$\frac{\partial b}{\partial t}(a, t) + \frac{\partial b}{\partial a}(a, t) = -(k_D + r_K(a, d))b, \quad a > 0,\ t > 0 \tag{7.1}$$

with the killing rate function r_K defined by

$$r_K(a, d) = \begin{cases} k_K, & a \le \delta d \\ 0, & a > \delta d \end{cases}$$

where k_K is the killing coefficient. Here k_D is the natural death rate, d is the given antimicrobial concentration and δ is an adjustable tolerance coefficient. For a fixed d value, a small δ means that the cells become tolerant at a relatively young age, and a large δ means that the cells become tolerant at a relatively old age. Eq. (7.1) is a linear wave equation for $a > 0, t > 0$, with characteristics emanating from positive a- and t-axes. It is supplied with the initial condition $b(a, 0) = b_0(a)$ and a birth boundary condition at $a = 0$ given by

$$b(0, t) = \int_0^\infty r_b(a, C)b(a, t)\mathrm{d}a$$

where r_b is a birth rate function depending on the cell's age a and the substrate's concentration C. The evolution of C is governed by the ODE

$$\frac{\mathrm{d}C}{\mathrm{d}t} = -\int_0^\infty r_C(a, C)b(a, t)\mathrm{d}a$$

where r_C is a substrate usage function. A typical numerical simulation [79] is shown in Fig. 11. It predicted the bi-phasic disinfection curve and the relative scarcity of persisters during the growth phase as opposed to during the stationary phase. Thus this model based on senescence provides a natural explanation for persistence-related phenomena.

7.3. Viscoelastic model

Towler et al. [80] developed a finite element model of the biofilm response to flows, in which a linear viscoelastic model (Burger material law) is coupled to finite element fluid solver sequentially to study the mechanical response of a single semi-spherical cluster to incompressible and turbulent flows. They concluded that the deformation paths of the viscoelastic biofilm are largely insensitive to the specific material coefficients in the model. Burger's material law is given by a linear integral constitutive equation:

$$\begin{aligned}\epsilon_{ij}(t) = \delta_{ij}\Bigg[\left(\frac{1}{R_1} - \frac{1}{G_1}\right)\sigma_{kk}(t) + \int_0^t \Bigg[-\frac{1}{G_2}(1 - \mathrm{e}^{-G_2(t-\tau)/\eta_2}) \\ - \frac{t-\tau}{\eta_1}\Bigg]\frac{\partial \sigma_{kk}}{\partial \tau}\Bigg] + \frac{1}{G_1}\sigma_{ij}(t) \\ + \int_0^t \left[\frac{1}{G_2}(1 - \mathrm{e}^{-G_2(t-\tau)/\eta_2}) + \frac{t-\tau}{\eta_1}\right]\frac{\partial \sigma_{ij}(\tau)}{\partial \tau}\mathrm{d}\tau,\end{aligned} \tag{7.2}$$

where ϵ is the train tensor, δ is the Kroneker delta, σ is the stress tensor, t is time, R_1 is the bulk elastic modulus, G_1 and η_1 are the shear modulus and viscous coefficient, respectively, for the Maxwell component of the Burger model, and G_2 and η_2 are the shear modulus and viscous coefficient, respectively for the Kelvin component. Essentially, the biofilm cluster is treated as a piece of the viscoelastic solid material in this model. Nonlinear viscoelastic models are developed in the context of one fluid multicomponent formulations, in which various viscoelastic constitutive equations can be incorporated depending on the microstructure of the EPS network [64,66].

7.4. Modeling biofilms using other computational cellular tools

[81] used the Glazier-Graner-Hogeweg (GGH) model coupled with a discrete-continuum model (PLH) developed by [52] to study the biofilm's dynamics provided by the CompuCell3D modeling environment, a cell-oriented framework designed to simulate the growth and the pattern formation due to the biological cells' behaviors. They simulated the growth of a single-species bacterial biofilm, and studied the roles of the cell-cell and the cell-flow-field interactions in determining the biofilm's morphology. In their simulations, which generalized the PLH model by treating cells as spatially extended deformable bodies, differential adhesion between cells and their competition for a substrate (nutrient), surface to produce a fingering instability that generates the finger shapes of biofilms.

8. Conclusion

We have revisited a few families of the biofilm models chronicologicaly. The models described in this review article have already been used to explain many complicated phenomena in the biofilm's dynamics. However, there are still many unanswered questions in the mathematical biofilm's modeling, especially in the effort of incorporating all the physical, chemical, biological and ecological processes occurring at various time- and length-scales into a comprehensive analytical or computational model. With the improvement on one's understanding of the biofilm's dynamics and fast advancing computing technology and experimental techniques, we anticipate another surge in research activities in this scientifically and technologically important and economically even more important topic. Due to the scope of the review, we left out some important issues such as quorum sensing etc.

Acknowledgement

Qi Wang acknowledges the partial support from the National Science Foundation through grants DMS-0605029, DMS-0626180, EPS-0447660, DMS-0819051 and DMS-0908330 as well as the startup fund from USC. He would like to thank Chern's Institute of Mathematics at Nankai University and Nankai Institute for Scientific Computing for their hospitality and support during his visit when this article was finalized. Partial support for Qi Wang's work from the Kavli Institute for Theoretical Physics China at Chinese Academy of Sciences is also greatly appreciated. Tianyu Zhang acknowledges the partial support from the startup fund from Montana State University.

References

[1] J.W. Costerton, Z. Lewandowski, D.E. Caldwell, D.R. Korber, H.M. Lappin-Scott, Annu. Review Microbiol. 49 (1995) 711–745.
[2] M.E. Davey, G.A. O'Toole, Microbiol. Mol. Biol. Rev. 64 (2000) 847–867.
[3] G.A. O'Toole, H.B. Kaplan, R. Kolter, Annu. Rev. Microbiol. 54 (2000) 49–79.
[4] C. Picioreanu, J.B. Xavier, M.C.M. van Loosdrecht, Biofilm 1 (2004) 337–349.
[5] B.E. Rittmann, P.L. McCarty, Biotech. Bioeng. 22 (1980) 2359–2373.
[6] B.E. Rittmann, P.L. McCarty, Biotech. Bioeng. 22 (1980) 2343–2357.
[7] B.E. Rittmann, Biotech. Bioeng. 24 (1982) 501–506.
[8] O. Wanner, W. Gujer, Wat. Sci. Tech. 17 (1984) 27–44.
[9] O. Wanner, W. Gujer, Wat. Sci. Tech. 28 (1986) 314–328.
[10] J.C. Kissel, P.L. McCarty, R.L. Street, J. Environ. Eng. 110 (1984) 393–411.
[11] O. Wanner, P. Riechert, Biotech. Bioeng. 49 (1996) 172–184.
[12] T.A. Witten, L.M. Sander, Phys. Rev. Lett. 47 (1981) 1400–1403.
[13] H. Fujikawa, M. Matsushita, J. Phys. Soc. Japan 58 (1989) 3875–3878.
[14] M. Matsushita, H. Fujikawa, Physica A 168 (1990) 498–506.
[15] H. Fujikawa, FEMS Microbiol. Ecol. 13 (1994) 159–168.
[16] S. Tolman, P. Meakin, M. Matsushita, J. Phy. Soc. Jpn. 58 (1989) 2721–2726.
[17] E.R. Berlekamp, J.H. Conway, R.K. Guy, Academic Press, New York, NY, 1982.
[18] S. Wolfram, Nature (London) 311 (1984) 419–424.
[19] D.G. Green, Math. Comp. Mod. 13 (1990) 69–74.
[20] G.B. Ermentrout, L. Edelstein-Keshet, J. Theoret. Biol. 160 (1993) 97–133.
[21] R.L. Colasanti, Binary Comput. Microbiol. 4 (1992) 191.
[22] G.C. Barker, M.J. Grimson, Binary Comput. Microbiol. 5 (1993) 132–137.
[23] E. Ben-Jacob, O. Schochet, A. Tenenbaum, I. Cohen, A. Czirok, V. Tamas, Nature (London) 368 (1994) 46–49.
[24] J.W.T. Wimpenny, R. Colasanti, FEMS Microbiol. Ecol. 22 (1997) 1–16.
[25] G. Pizarro, D. Griffeath, D.R. Noguera, J. Environ. Eng. 127 (2001) 782–789.
[26] G. Pizarro, C. Garcia, R. Moreno, M.E. Sepulveda, Wat. Sci. Tech. 49 (2004) 193–198.
[27] C. Picioreanu, M.C.M. Loosdrecht, J.J. Heijnen, Biotech. Bioeng. 57 (1998) 718–731.
[28] R.H. Wijffels, C.D. de Gooijer, S. Kortekass, J. Tramper, Biotech. Bioeng. 38 (1991) 224–231.
[29] R.H. Wijffels, C.D. de Gooijer, S. Kortekass, J. Tramper, Biotech. Bioeng. 38 (1991) 232–240.
[30] R.H. Wijffels, Ph.D. Thesis, Wageningen Agricultural University, Wageningen, The Netherlands, 1994.
[31] D.R. Noguera, G. Pizarro, D.A. Stahl, B.E. Rittman, Wat. Sci. Tech. 39 (1999) 123–130.
[32] S.W. Hermanowicz, Math. Biosci. 169 (2001) 1–14.
[33] D. DeBeer, P. Stoodely, Z. Lewandowski, Biotech. Bioeng. 44 (1994) 636–641.
[34] D. DeBeer, P. Stoodely, Z. Lewandowski, Water Res. 30 (1996) 2761–2765.
[35] D. DeBeer, P. Stoodely, F. Roe, Z. Lewandowski, Biotech. Bioeng. 43 (1994) 1131–1138.
[36] S.M. Hunt, M.A. Hamilton, J.T. Sears, G. Harkin, J. Reno, Microbiology 149 (2003) 1155–1163.
[37] S.M. Hunt, E.M. Werner, B. Huang, M.A. Hamilton, P.S. Stewart, Appl. Environ. Microbiol. 72 (2004) 7418–7425.
[38] J.D. Chambless, P.S. Stewart, Biotech. Bioeng. 97 (2007) 1573–1584.
[39] J.D. Chambless, S.M. Hunt, P.S. Stewart, Appl. Environ. Microbiol. 72 (2006) 2005–2013.
[40] A. Gjaltema, P.A.M. Arts, M.C.M. van Loosdrecht, J.G. Kuenen, J.J. Heijnen, Biotech. Bioeng. 44 (1994) 194–204.
[41] T.C. Zhang, P.L. Bishop, Water Res. 28 (1994) 2267–2277.
[42] T.C. Zhang, P.L. Bishop, Water Res. 28 (1994) 2279–2287.
[43] P. Stoodley, Z. Lewandowski, J.D. Boyle, H.M. Lappin-Scott, Biotech. Bioeng. 65 (1999) 83–92.
[44] P. Stoodley, Z. Lewandowski, J.D. Boyle, H.M. Lappin-Scott, Environ. Microbiol. 1 (1999) 447–457.
[45] P. Stoodley, F. Jorgensen, P. Williams, H.M. Lappin-Scott, in: R. Bayston, et al. (Eds.), Biofilms: The Good, The Bad, and The Ugly, Bioline Press, Cardiff, United Kingdom, 1999, pp. 323–330.
[46] C. Picioreanu, M.C. Loosdrecht, J.J. Heijnen, Wat. Sci. Tech. 39 (1999) 115–122.
[47] C. Picioreanu, M.C. Loosdrecht, J.J. Heijnen, Biotech. Bioeng. 69 (2000) 504–515.
[48] C. Picioreanu, M.C. Loosdrecht, J.J. Heijnen, Biotech. Bioeng. 72 (2001) 205–218.
[49] S.P. Dawson, S. Chen, G.D. Doolen, J. Chem. Phys. 98 (1993) 1514–1523.
[50] S. Chen, S.P. Dawson, G.D. Doolen, D.R. Janecky, A. Lawniczak, Computers Chem. Engng. 19 (1995) 617–646.
[51] Y. Chen, H. Ohashi, M. Akiyama, JSME Int. J. Series B 40 (1997) 25–32.
[52] C. Picioreanu, M.C. Loosdrecht, J.J. Heijnen, Biotech. Bioeng. 58 (1998) 101–116.
[53] R. Dillon, L. Fauci, A. Fogelson, D. Gaver, J. Comput. Phys. 129 (1996) 57–73.
[54] R. Dillon, L. Fauci, Biotech. Bioeng. 68 (2000) 536–547.
[55] H.J. Eberl, D.F. Parker, M.C.M. van Loosdrecht, J. Theoret. Med. 3 (2001) 161–175.
[56] J. Dockery, I. Klapper, SIAM. J. Appl. Math. 62 (2001) 853–869.
[57] E. Alpkvist, I. Klapper, Bull. Math. Biol. 69 (2007) 765–789.
[58] N.G. Cogan, J.P. Keener, Math. Med. Biol. 21 (2004) 147–166.
[59] A.N. Beris, B. Edwards, Thermodynamics of Flowing System, Oxford University Press, 1994.
[60] C.A. Fux, S. Wilson, P. Stoodley, J. Bacteriol. 186 (2004) 4486–4491.
[61] I. Klapper, J. Dockery, Phys. Rev. E 74 (2006) 031902.
[62] B.W. Towler, C.R. Rupp, A. Cunningham, P. Stoodley, Biofouling 19 (2003) 279–285.
[63] I. Klapper, C.J. Rupp, R. Cargo, B. Purevdorj, P. Stoodly, Biotech. Bioeng. 80 (2002) 289–296.
[64] T. Zhang, N. Cogan, Q. Wang, SIAM, J. Appl. Math. 69 (2008) 641–669.
[65] T. Zhang, N. Cogan, Q. Wang, Commun. Comput. Phys. 4 (2008) 72–101.
[66] Q. Wang, T. Zhang, Discrete and Continuous Dynamical Systems: Series B (2010) (in revision).
[67] J.-U. Kreft, G. Booth, J.W.T. Wimpenny, Microbiology 144 (1998) 3275–3287.
[68] J.-U. Kreft, C. Picioreanu, J.W.T. Wimpenny, M.C.M. van Loosdrecht, Microbiology 147 (2001) 2897–2912.
[69] C. Picioreanu, J.-U. Kreft, M.C. Loosdrecht, Appl. Environ. Microbiol. 70 (2004) 3024–3040.
[70] C.A. Gordon, N.A. Hodges, C. Marriot, J. Antimicrob. Chemother. 22 (1988) 667–674.
[71] W.W. Nichols, S.M. Dorrington, M.P.E. Slack, H.L. Walmsley, Antimicrob. Agents Chemother. 32 (1988) 518–523.
[72] D. DeBeer, R. Srinivasan, P.S. Stewart, Appl. Environ. Microbiol. 60 (1994) 4339–4344.
[73] P.S. Stewart, J. Raquepas, Chem. Eng. Sci. 50 (1995) 3099–3104.
[74] P.S. Stewart, Antimicrob. Agents Chemother. 40 (1996) 2517–2522.
[75] P.S. Stewart, Internatl. J. Med. Microbiol. 292 (2002) 107–113.
[76] K. Lewis, Antimicrob. Agents Chemother. 45 (2001) 999–1007.
[77] I. Keren, N. Kaldalu, A. Spoering, Y. Wang, K. Lewis, FEMS Microbiol. Lett. 230 (2004) 13–18.
[78] N.G. Cogan, J. Theoret. Biol. 238 (2006) 694–703.
[79] I. Klapper, P. Gilbert, B.P. Ayati, J. Dockery, P.S. Stewart, Microbiology 153 (2007) 3623–3630.
[80] B.W. Towler, A. Cunningham, P. Stoodley, L. McKittrick, Biotech. Bioeng. 96 (2007) 259–271.
[81] N.J. Poplawski, A. Shirinifard, M. Swat, J.A. Glazier, Math. Biosciences Eng. 8 (2008) 355–388.